Self-consistent description of single-particle levels of magic nuclei

N. V. Gnezdilov
Kurchatov Institute, 123182 Moscow, Russia, and National Research Nuclear University MEPhI, 115409 Moscow, Russia

I. N. Borzov
Institute for Physics and Power Engineering, 249033 Obninsk, Russia, and Joint Institute for Nuclear Research, 141980 Dubna, Russia

E. E. Saperstein
Kurchatov Institute, 123182 Moscow, Russia

S. V. Tolokonnikov
Kurchatov Institute, 123182 Moscow, Russia, and Moscow Institute of Physics and Technology, 141700 Dolgoprudny, Russia

(Received 8 January 2014; revised manuscript received 10 February 2014; published 11 March 2014)

Single-particle levels of seven magic nuclei are calculated within the energy density functional (EDF) method by Fayans *et al*. [Nucl. Phys. A **676**, 49 (2000)]. Three versions of the EDF are used, the initial Fayans functional, DF3, and its two variations, DF3-a and DF3-b, with different values of spin-orbit parameters. Comparison is made with predictions of the Skyrme-Hartree-Fock method with the HFB-17 functional. For the DF3-a functional, phonon coupling (PC) corrections to single-particle energies are found self-consistently with an approximate account for the tadpole diagram. Accounting for the PC corrections improves the agreement with the data for heavy nuclei, e.g., for ^{208}Pb. On the other hand, for lighter nuclei, e.g., ^{40,48}Ca, PC corrections make the agreement a little worse. As estimations show, the main reason is that the approximation we use for the tadpole term is less accurate for light nuclei.

DOI: 10.1103/PhysRevC.89.034304 PACS number(s): 21.60.Jz, 21.10.Ky, 21.10.Ft, 21.10.Re

I. INTRODUCTION

In the seminal article [1] on the Hartree-Fock (HF) method with effective forces, Vautherin and Brink reduced the effective Skyrme forces containing a three-body term to a much simpler version with a density-dependent two-body force. Initially, this dependence was assumed to be linear, just as that of the scalar Landau-Migdal interaction amplitude in the theory of finite Fermi systems (TFFS) [2] playing the role of the effective interaction in this approach. Inclusion of a velocity-dependent force is another essential feature of the Skyrme HF (SHF) method. As a result, the SHF effective Hamiltonian $\mathcal{H}_{\rm SHF}$ will involve, in addition to the neutron and proton densities $\rho_{n,p}(\mathbf{r})$, the kinetic energy densities $\tau_{n,p}(\mathbf{r})$. The coordinate-dependent effective masses $m^*_{n,p}(r)$, as a rule, differ significantly from the free-nucleon mass m. At first sight, this structure of the effective Hamiltonian seems to contradict the Hohenberg-Kohn theorem [3], which states that the ground-state energy of a Fermi system E_0 is a functional of the density $\rho(\mathbf{r})$. However, as shown, e.g., in [4], the kinetic energy $\tau(\mathbf{r})$ can be expressed in terms of the density $\rho(\mathbf{r})$, although the relation is rather complicated.

Due to its simplicity, the SHF method quickly became very popular and up to now it dominates the self-consistent description of nuclear properties. From the very beginning, the SHF method was aimed at calculating global properties of nuclei, such as the binding energy and average radii. There are numerous sets of Skyrme force parameters, some of them resulting in the description of nuclear masses with a high accuracy. The set HFB-17 [5] led to a record accuracy which is better, on average, than 600 keV. We compare our results for single-particle spectra we analyze with those obtained with the HFB-17 functional.

At the same time, from the very beginning, the SHF method turned out to be unsuccessful in describing single-particle spectra produced by SHF mean-field potentials. The reason was the significant deviation of the effective masses $m^*_{n,p}(r = 0) \simeq 0.6 \div 0.8m$ from the bare one typical for the SHF approach. In fact, the simplest shell model with Saxon-Woods potentials and $m^* = m$ was, as a rule, more successful at this point. It is noteworthy that the inclusion of single-particle energies to the fit of the SHF parameters [6] led to an effective mass close to the bare one.

A bit later the self-consistent TFFS was developed. It was based on the basic principles of the TFFS [2] supplemented with the condition of self-consistency in the TFFS among the energy-dependent mass operator $\Sigma(\mathbf{r_1},\mathbf{r_2};\varepsilon)$, the single-particle Green function $G(\mathbf{r_1},\mathbf{r_2};\varepsilon)$, and the effective nucleon-nucleon interaction $\mathcal{U}(\mathbf{r_1},\mathbf{r_2},\mathbf{r_3},\mathbf{r_4};\varepsilon,\varepsilon')$ [7]. The final version of this approach [8–10] was formulated in terms of the quasiparticle Lagrangian $\mathcal{L}_q$, which is constructed to produce the quasiparticle mass operator $\Sigma_q(\mathbf{r},k^2;\varepsilon)$. By definition, the latter coincides at the Fermi surface with the exact mass operator $\Sigma(\mathbf{r},k^2;\varepsilon)$. In the mixed coordinate-momentum representation it depends linearly on the momentum squared k^2 and the energy ε as well [2]. In magic nuclei which are nonsuperfluid, the Lagrangian $\mathcal{L}_q$ depends on three sorts of densities $\nu_i(\mathbf{r})$, $i = 0,1,2$. The first two densities are analogs of the SHF densities $\rho(\mathbf{r})$ and $\tau(\mathbf{r})$, whereas the density $\nu_2(\mathbf{r})$ is a new ingredient of the self-consistent theory. It is the density of single-particle energies which appears naturally due to the ε dependence of the quasiparticle mass operator and determines

the Z factor

$$Z(\mathbf{r}) = \frac{1}{1 - \left(\frac{\partial \Sigma}{\partial \varepsilon}\right)_0}, \tag{1}$$

where the index 0 means that the energy and momentum variables are taken at the Fermi surface.

The self-consistent TFFS permits us to obtain the same bulk nuclear characteristics as the SHF method. In addition, it helps to find the Z factor, which determines the in-volume component of the one-nucleon S factors. On equal footing, the TFFS from the very beginning was focused on the analysis of single-particle spectra. The effective mass appearing in this approach contains not only the so-called k mass, as in the SHF method, but also the "E mass":

$$\frac{m}{m^*(\mathbf{r})} = Z(\mathbf{r})\left[1 + 2m\left(\frac{\partial \Sigma}{\partial k^2}\right)_0\right]. \tag{2}$$

As found in [9], these two ingredients of the effective mass should strongly cancel each other in order to describe the single-particle spectra of magic nuclei. The optimal set of parameters found in [9] corresponds to the following characteristics of nuclear matter: $Z_0 = 0.8$, $m_n^* = 0.95$, $m_p^* = 1.05$, which explains the success of the shell model with $m^* = m$. For nuclear matter, a strong cancellation of the k mass and E mass is well known in the Bruekner theory. It was also analyzed within the relativistic Bruekner-HF method in Ref. [11].

It is noteworthy that corrections to the mean-field theory due to contributions of the low-lying surface vibrations, "phonons," were involved in the analysis in [9]. All phonon coupling (PC) diagrams were taken into account, including so-called tadpole terms. The method developed by Khodel [12] was used at that point.

Again, as in the SHF theory case, the appearance of a new density $\nu_2(\mathbf{r})$ does not contradict the Hohenberg-Kohn theorem. As found in [13], it can be excluded if one goes from the quasiparticle Lagrangian $\mathcal{L}_q$ to the quasiparticle Hamiltonian $\mathcal{H}_q$, which depends now on two densities, just as the SHF Hamiltonian $\mathcal{H}_{\mathrm{SHF}}$. Moreover, if, on the basis of the closeness of the neutron and proton effective masses to the bare one, we put $m_n^* = m_p^* = m$, the Hamiltonian $\mathcal{H}_q$ will depend only on the density $\rho(\mathbf{r})$ normalized in a standard way, just as in the energy density functional (EDF) of Kohn-Sham [14]. However, the quasiparticle Lagrangian of rather simple structure introduced in [9] leads to a very complicated density dependence of the Hamiltonian $\mathcal{H}_q[\rho(\mathbf{r})]$ [13] which could hardly be introduced *ad hoc*.

The next important step in the self-consistent TFFS was made by Fayans and coauthors [15]. On the base of the analysis in [13], they formulated the theory directly in terms of the EDF approach. They generalized the Kohn-Sham method to superfluid systems, proposing for the normal component of the EDF the fractional density dependence, with finite-range force,

$$E_0 = \int C_0 a\, f(|\mathbf{r} - \mathbf{r}'|)\frac{\rho(\mathbf{r}')^2}{2}\frac{1 - h_1(\rho(\mathbf{r}')/\rho_0)^\alpha}{1 + h_2\rho(\mathbf{r}')/\rho_0}\, d^3r\, d^3r', \tag{3}$$

where the factor $C_0 = (dn/d\varepsilon_{\mathrm{F}})^{-1}$ is the usual TFFS normalization factor, the inverse density of states at the Fermi surface, and ρ_0 is the nuclear matter density. The constants a, h_1, h_2, ρ_0, and α are parameters and the Yukawa form for the finite-range function $f(r)$ was used. Isotopic indices in (3) are omitted for brevity. In Eq. (3), the spin-orbit and Coulomb interaction for protons are omitted as well. For nuclear matter, the EDF, (3), with parameter values of [15] turned out to be very close to that in [13]. The identity $m^* = m$, which is a usual feature of the Kohn-Sham method, was proposed in this approach. The explicit form of the Fayans EDF and its different parametrizations DF1–DF3 can be found in [16], [17], or [18].

Recently, new data on single-particle spectra appeared [19] for seven magic nuclei, from ^{40}Ca to ^{208}Pb. For two of them, ^{78}Ni and ^{100}Sn, the spectra were not measured directly but were interpolated from the neighboring nuclei. The bulk of these data contains 35 spin-orbit energy differences, which can be used for fitting the spin-orbit and effective tensor force parameters. In this article we carry out a comparative analysis of these spectra within the EDF approach of Fayans *et al.* and the SHF method with the set HFB-17 [5].

In addition, we analyze the PC corrections to single-particle spectra including the tadpole term. The particle-vibration coupling was extensively studied within the so-called quasiparticle-phonon model of Soloviev [20] and within the "nuclear -field" approach of Bortignon and Broglia [21]. The use of phenomenological parameters for single-particle spectra and particle-PC constants was typical for these approaches. Evidently, the first self-consistent consideration of the PC corrections to the single-particle spectra was made by Bernard and Nguyen [22] within the SHF method. However, for a long time this approach has been abandoned. Recently the interest in this problem has been renewed. Self-consistent calculations with the SHF functionals have been carried out in [23] within the quasiparticle-phonon model and in [24–26] within the nuclear-field method. In a recent article [27] this problem was attacked within the relativistic mean-field (RMF) theory (see [28], and references therein).

Within the TFFS, the problem of PC corrections to ε_λ was examined in very old articles [9,29]. An important feature of these calculations was accounting for so-called tadpole diagrams, which are ignored in all the approaches mentioned above. The method developed by Khodel [12] is used for this aim. However, these calculations were not completely self-consistent. They used the Saxon-Woods basis, and the TFFS self-consistency relation [7] was taken into account approximately. In this article, we follow the approach of [9] and [29], enabling complete self-consistency, i.e., with the self-consistent basis and self-consistent finding of the PC vertices g_L for each of the L phonons. In addition, a wider number of magic nuclei is considered for which single-particle spectra are available.

II. EDF DESCRIPTION OF SINGLE-PARTICLE LEVELS

The parameter set DF3 [16] was used in the vest-known application of the generalized EDF method of Fayans *et al.* [17]. This set not only was fitted to characteristics of stable

TABLE I. Spin-orbit parameters of different versions of the Fayans EDF.

Parameter	DF3 [17]	DF3-a [30]	DF3-b
κ	0.216	0.190	0.165
κ'	0.077	0.077	0.075
g_1	0	0	−0.100
g_1'	−0.123	−0.308	−0.300

spherical nuclei from calcium to lead but also was specially fitted to single-particle levels of the very neutron-rich doubly magic nucleus ^{132}Sn. In Ref. [30], it was applied to nuclei of uranium and transuranium regions which had not been analyzed previously within this approach. It was found that for successful description of this new bulk of nuclei, the spin-orbit parameters of the basic DF3 set should be modified. To compare these two functionals explicitly, we write down the spin-orbit terms of the EDF we discuss.

The main spin-orbit effective interaction is taken in [16] and [17] in the usual TFFS form,

$$\mathcal{F}_{sl} = C_0 r_0^2(\kappa + \kappa'\boldsymbol{\tau}_1\boldsymbol{\tau}_2)[\nabla_1\delta(\mathbf{r}_1 - \mathbf{r}_2) \times (\mathbf{p}_1 - \mathbf{p}_2)] \cdot (\boldsymbol{\sigma}_1 + \boldsymbol{\sigma}_2), \quad (4)$$

with obvious notation. Here the factor r_0^2 is introduced to make the spin-orbit parameters κ and κ' dimensionless. It can be expressed in terms of the equilibrium density ρ_0 of nuclear matter introduced above, $r_0^2 = (3/(8\pi\rho_0))^{2/3}$.

In nuclei with partially occupied spin-orbit doublets, the so-called spin-orbit density exists,

$$\rho_{sl}^{\tau}(\mathbf{r}) = \sum_{\lambda} \mathbf{n}_{\lambda}^{\tau}\left\langle\phi_{\lambda}^{\tau *}(\mathbf{r})(\boldsymbol{\sigma}\mathbf{l})\phi_{\lambda}^{\tau}(\mathbf{r})\right\rangle, \quad (5)$$

where $\tau = n, p$ is the isotopic index and averaging over spin variables is carried out. As is well known (see, e.g., [9]), a new term appears in the spin-orbit mean field induced by the tensor forces and the first harmonic $\hat{g_1}$ of the spin Landau-Migdal amplitude. We combine those contributions into an effective tensor force or first spin harmonic:

$$\mathcal{F}_1^s = C_0 r_0^2(g_1 + g_1'\boldsymbol{\tau}_1\boldsymbol{\tau}_2)\delta(\mathbf{r}_1 - \mathbf{r}_2)(\boldsymbol{\sigma}_1\boldsymbol{\sigma}_2)(\mathbf{p}_1\mathbf{p}_2). \quad (6)$$

For brevity, we call all four parameters in Eqs. (4) and (6) spin-orbit parameters.

The spin-orbit parameters of the set in [30] called DF3-a are listed in Table I, together with the initial set DF3. Also, a new set, DF3-b, has been found for optimal description of the spin-orbit energy differences. In Ref. [19] the bulk of the data is given on spin-orbit doublets with known values of the energies of both components, the total number being 35. This provides us with the possibility of such optimization. The experimental values of the spin-orbit differences, $\Delta_{nls} = \varepsilon_{n,l,j=l-1/2} - \varepsilon_{n,l,j=l+1/2}$, for all magic nuclei are listed in Table II together with predictions of the different functionals we analyze. For comparison with the SHF method, we calculated also the single-particle spectra with the HFB-17 functional [5]. To characterize the accuracy of all named functionals in describing this specific set of data we found the average theoretical error of predictions for each of them

TABLE II. Deviations $\delta\Delta_{nls}$ (MeV) of the theory predictions $\Delta_{\rm nls}^{\rm theor}$ for spin-orbit differences from experimental values for different functionals.

Nucleus	λ	$\Delta_{nls}^{\rm exp}$	$\Delta_{nls}^{\rm theor} - \Delta_{nls}^{\rm exp}$			
			DF3-b	DF3-a	DF3	HFB-17
^{40}Ca-p	$1f$	5.69	0.69	1.43	2.29	3.57
	$1d$	5.40	−0.40	0.22	0.90	2.35
	$2p$	1.75	−0.35	−0.16	0.02	0.26
^{40}Ca-n	$1f$	5.71	0.99	1.80	2.71	4.24
	$1d$	5.63	−0.50	0.12	0.82	2.34
	$2p$	2.00	−0.34	−0.12	0.09	0.46
^{48}Ca-p	$1f$	5.08	0.46	0.84	2.87	5.05
	$1d$	5.77	−2.18	−1.98	−0.42	1.50
	$2p$	1.50	−0.41	−0.29	0.03	0.70
^{48}Ca-n	$1f$	8.75	−0.13	0.21	0.39	1.47
	$2p$	2.03	−0.24	−0.13	−0.22	0.21
^{56}Ni-p	$1f$	7.45	−0.49	−0.56	0.83	2.49
	$2p$	1.11	0.21	0.20	0.17	0.78
^{56}Ni-n	$1f$	7.17	0.14	0.06	1.41	3.16
	$2p$	1.11	0.39	0.39	0.37	1.02
^{78}Ni-p	$1f$	5.12	0.17	0.09	1.07	2.77
	$2p$	1.40	−0.11	−0.05	−0.05	0.41
^{78}Ni-n	$2p$	1.33	0.02	0.06	0.22	0.80
^{100}Sn-p	$1g$	6.86	−0.44	−0.50	0.69	2.60
	$2p$	1.10	0.15	0.20	0.27	0.74
^{100}Sn-n	$1g$	6.35	0.41	0.32	1.45	3.42
	$2d$	1.57	0.49	0.57	0.66	1.41
^{132}Sn-p	$1g$	6.13	−1.11	−1.17	−0.27	1.48
	$2d$	1.74	−0.02	0.08	0.19	0.82
^{132}Sn-n	$1h$	6.75	0.90	0.92	1.82	3.76
	$2f$	2.01	0.01	0.05	0.44	1.30
	$3p$	0.80	−0.36	−0.35	−0.31	0.32
^{208}Pb-p	$1h$	5.56	−0.95	−0.96	−0.17	1.54
	$2f$	1.92	−0.01	0.15	0.31	1.06
	$2d$	1.34	0.05	0.17	0.31	0.86
	$3p$	0.85	−0.16	−0.09	−0.02	0.21
^{208}Pb-n	$1i$	5.84	1.05	1.03	1.83	3.82
	$2g$	2.49	−0.02	0.12	0.42	1.51
	$2f$	1.77	0.38	0.53	0.81	1.68
	$3d$	0.97	−0.15	−0.09	0.00	0.83
$\langle\delta\Delta_{nls}\rangle_{\rm rms}$			0.60	0.68	1.04	2.16

with the expression

$$\langle\delta\Delta_{nls}\rangle_{\rm rms} = \sqrt{\frac{1}{N}\sum_{i=1}^{N}\left(\Delta_{nls,i}^{\rm theor} - \Delta_{nls,i}^{\rm exp}\right)^2}, \quad (7)$$

with obvious notation. The average error values are listed in the last row in Table II. Indeed, the DF3-b version wins the competition. The DF3-a functional describes the spin-orbit doublets a little more poorly. For the DF3 version, the error increases to 1 MeV, which is, however, twice as low as the HFB-17 result.

In Figs. 1–14 we compare the experimental data [19] with our calculations employing three versions of the DF3 functional and using the SHF functional HFB-17. To characterize

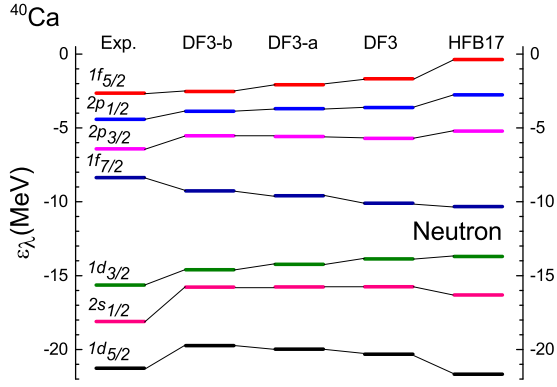

FIG. 1. (Color online) Neutron single-particle levels in ^{40}Ca. Experimental data from [19].

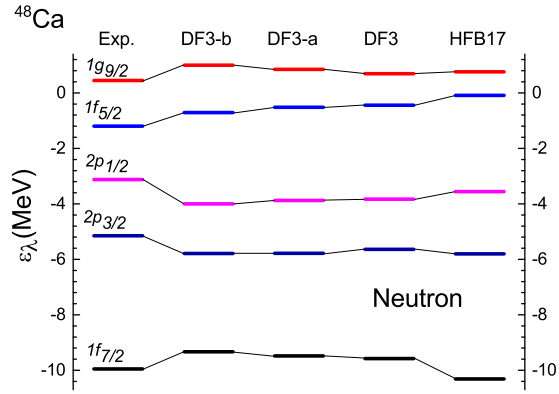

FIG. 3. (Color online) Neutron single-particle levels in ^{48}Ca. Experimental data from [19].

the accuracy of a specific version, on average, we calculated the corresponding average deviation of the theoretical predictions from experiment for each magic nucleus,

$$\langle \delta\varepsilon_\lambda \rangle_{\rm rms} = \sqrt{\frac{1}{N}\sum_\lambda \left(\varepsilon_\lambda^{\rm theor} - \varepsilon_\lambda^{\rm exp}\right)^2}; \qquad (8)$$

the summation involves both neutrons and protons. The results are listed in Table III. The last row reports results of summation over all nuclei. We see that the accuracy of all three versions of the DF3 functional is significantly higher than that of the HFB-17 functional. We explain this with two important features of the Fayans approach. First, it is the use of the bare mass $m^* = m$, which is close to the prescription $m^*/m = 1 \pm 0.05$ of [9]. Second, the density dependence of the Fayans EDF, (3), is essentially more sophisticated than the SHF one. Being rather close to that in [13], it involves implicitly the energy dependence of the quasiparticle mass operator within the TFFS. Evidently, SHF functionals turn out to be oversimplified for describing successfully nuclear characteristics finer than the binding energies.

Among the three versions of the DF3 functionals, the accuracy of the original one for spectra of magic nuclei is a little higher. However, the set DF3-a proved to be rather successful, better than DF3, in describing characteristics of semimagic nuclei such as the excitation energies and $B(E2)$ values of the first 2^+ states in even nuclei [18,31] and quadrupole moments of odd semimagic nuclei [32,33]. All these quantities are very sensitive to the position of single-particle levels in the vicinity of the Fermi surface. In addition, as mentioned above, the DF3-a functional works better for nuclei heavier than lead. Therefore in the next section, dealing with PC corrections to single-particle spectra, we use the DF3-a functional.

III. PHONON COUPLING CORRECTIONS TO SINGLE-PARTICLE ENERGIES

Accounting for PC effects, the equation for single-particle energies and wave functions can be written as

$$(\varepsilon - H_0 - \delta\Sigma^{\rm PC}(\varepsilon))\phi = 0, \qquad (9)$$

where H_0 is the quasiparticle Hamiltonian with the spectrum $\varepsilon_\lambda^{(0)}$ and $\delta\Sigma^{\rm PC}$ is the PC correction to the quasiparticle mass operator. After expanding this term in the vicinity of $\varepsilon = \varepsilon_\lambda^{(0)}$ one finds

$$\varepsilon_\lambda = \varepsilon_\lambda^{(0)} + Z_\lambda^{\rm PC}\delta\Sigma_{\lambda\lambda}^{\rm PC}\left(\varepsilon_\lambda^{(0)}\right), \qquad (10)$$

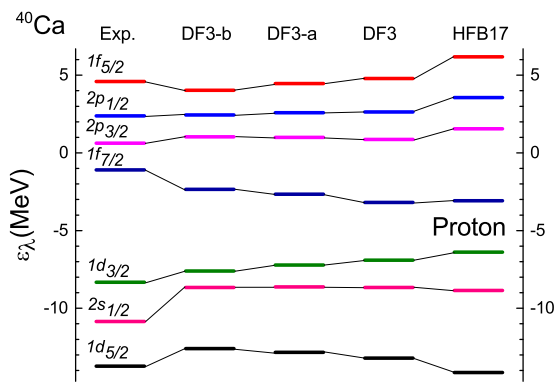

FIG. 2. (Color online) Proton single-particle levels in ^{40}Ca. Experimental data from [19].

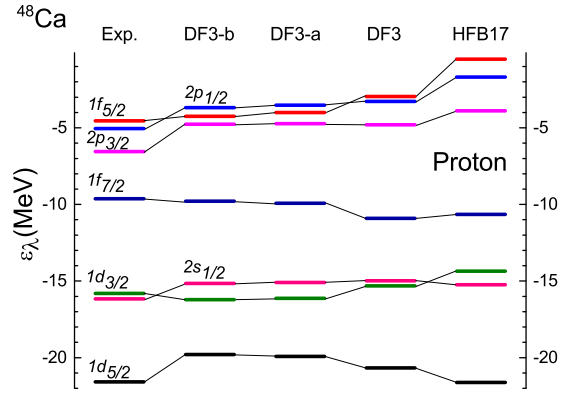

FIG. 4. (Color online) Proton single-particle levels in ^{48}Ca. Experimental data from [19].

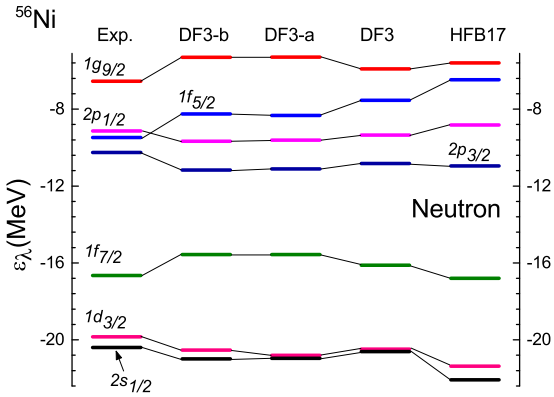

FIG. 5. (Color online) Neutron single-particle levels in ^{56}Ni. Experimental data from [19].

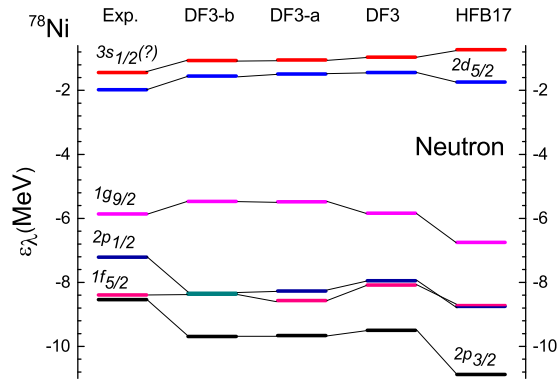

FIG. 7. (Color online) Neutron single-particle levels in ^{78}Ni. Experimental values [19] are interpolated from data for neighboring nuclei.

with obvious notation. Here $Z^{\rm PC}$ denotes the Z factor due to the PC effects, i.e., that found from Eq. (1) with substitution of $\delta\Sigma^{\rm PC}(\varepsilon)$ instead of the main mass operator $\Sigma(\varepsilon)$. Remember that in the TFFS the corresponding Z factor is included in the quasiparticle Hamiltonian H_0. For brevity, below the superscript PC is omitted. Expression (10) corresponds to the perturbation theory in the $\delta\Sigma$ operator with respect to H_0. In this article, we limit ourselves to magic nuclei where the so-called g_L^2 approximation, g_L being the L-phonon creation amplitude, is, as a rule, valid. It is worth mentioning that Eq. (10) is more general, including, say, g_L^4 terms.

Let us now consider g_L^2 corrections to the quasiparticle mass operator (Fig. 15). The first, pole diagram is well examined and corresponding equations can be found in textbooks, e.g., in [2] and [10]. Therefore we concentrate mainly on the second, tadpole term, which has not been as widely discussed in the literature.

The vertex g_L in Fig. 15 obeys the equation [2]

$$g_L(\omega) = \mathcal{F}A(\omega)g_L(\omega), \tag{11}$$

where $A(\omega) = \int G(\varepsilon+\omega/2)\,G(\varepsilon-\omega/2)\,d\varepsilon/(2\pi i)$ is the particle-hole propagator, $G(\varepsilon)$ being the one-particle Green function. In obvious symbolic notation, the pole diagram corresponds to $\delta\Sigma^{\rm pole} = (g_L, DGg_L)$, where $D_L(\omega)$ is the phonon D function, or explicitly one obtains

$$\delta\Sigma^{\rm pole}_{\lambda\lambda}(\epsilon) = \sum_{\lambda_1 M} |\langle\lambda_1|g_{LM}|\lambda\rangle|^2 \times \left(\frac{n_{\lambda_1}}{\varepsilon+\omega_L-\varepsilon_{\lambda_1}} + \frac{1-n_{\lambda_1}}{\varepsilon-\omega_L-\varepsilon_{\lambda_1}}\right), \tag{12}$$

where ω_L is the excitation energy of the L phonon and $n_\lambda = (0,1)$ stands for the occupation numbers.

All the low-lying phonons we consider have natural parity. In this case, the vertex g_L possesses even T parity. It is a sum of two components with spins $S=0$ and $S=1$, respectively,

$$g_L = g_{L0}(r)T_{LL0}(\mathbf{n},\alpha) + g_{L1}(r)T_{LL1}(\mathbf{n},\alpha), \tag{13}$$

where T_{JLS} stand for the usual spin-angular tensor operators [34]. The operators T_{LL0} and T_{LL1} have opposite T parities, hence the spin component should be the odd function of the excitation energy, $g_{L1} \propto \omega_L$. For the ghost dipole, $L=1$ and $\omega_1 = 0$, Eq. (11), due to the TFFS self-consistency relation [7], has the exact solution

$$g_1(\mathbf{r}) = \alpha_1 \frac{dU(r)}{dr} Y_{1M}(\mathbf{n}), \tag{14}$$

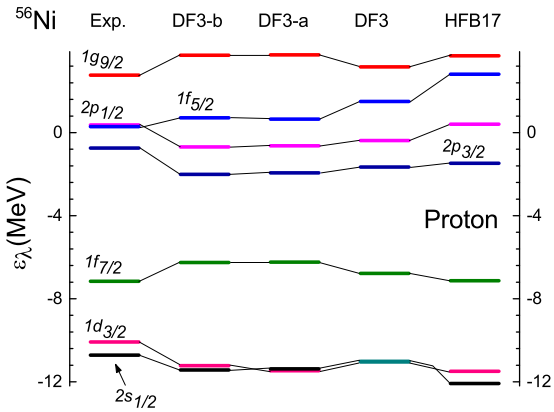

FIG. 6. (Color online) Proton single-particle levels in ^{56}Ni. Experimental data from [19].

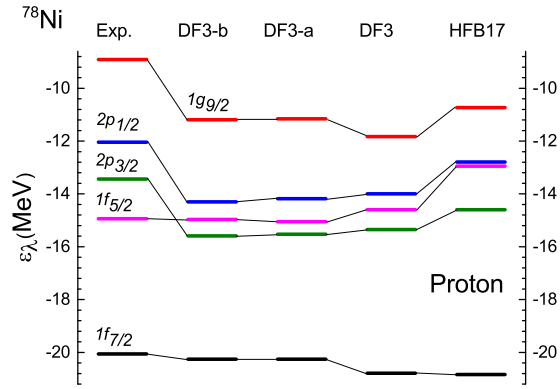

FIG. 8. (Color online) Proton single-particle levels in ^{78}Ni. Experimental values [19] are interpolated from data for neighboring nuclei.

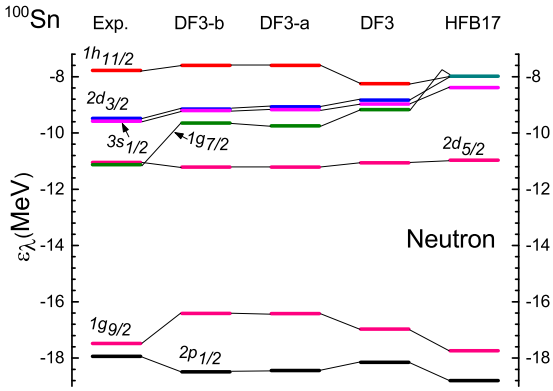

FIG. 9. (Color online) Neutron single-particle levels in ^{100}Sn. Experimental values [19] are interpolated from data for neighboring nuclei.

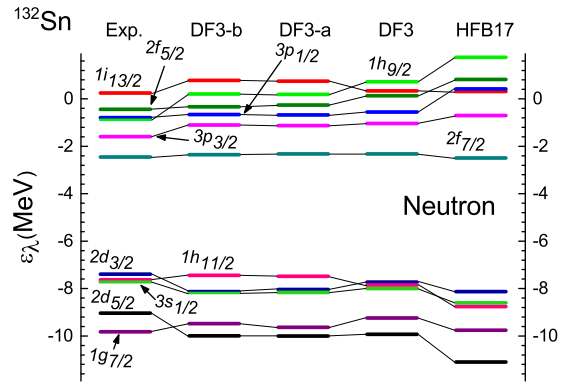

FIG. 11. (Color online) Neutron single-particle levels in ^{132}Sn. Experimental data from [19].

where $\alpha_1 = 1/\sqrt{2\omega B_1}$, $B_1 = 3mA/4\pi$ is the Bohr-Mottelson (BM) mass coefficient [35] and $U(r)$ is the central part of the mean-field potential generated by the energy functional.

For the ghost phonon it is convenient to rewrite Eq. (12) as follows:

$$\delta\Sigma^{\rm pole}_{\lambda\lambda}(\epsilon) = \alpha_1^2 \sum_{\lambda_1 M} \left| \langle \lambda_1 | \frac{dU}{dr} Y_{1M} | \lambda \rangle \right|^2 \times \left(\frac{\varepsilon - \varepsilon_{\lambda_1}}{\left(\varepsilon - \varepsilon_{\lambda_1}\right)^2 - \omega_1^2} + \omega_1 \frac{1 - 2n_{\lambda_1}}{\left(\varepsilon - \varepsilon_{\lambda_1}\right)^2 - \omega_1^2} \right). \quad (15)$$

The second, tadpole, term in Fig. 15 is

$$\delta\Sigma^{\rm tad} = \int \frac{d\omega}{2\pi i} \delta_L g_L D_L(\omega), \quad (16)$$

where $\delta_L g_L$ can be found [9,12] by variation of Eq. (11) in the field of the L phonon:

$$\delta_L g_L = \delta_L \mathcal{F} A(\omega_L) g_L + \mathcal{F} \delta_L A(\omega_L) g_L + \mathcal{F} A(\omega_L) \delta_L g_L. \quad (17)$$

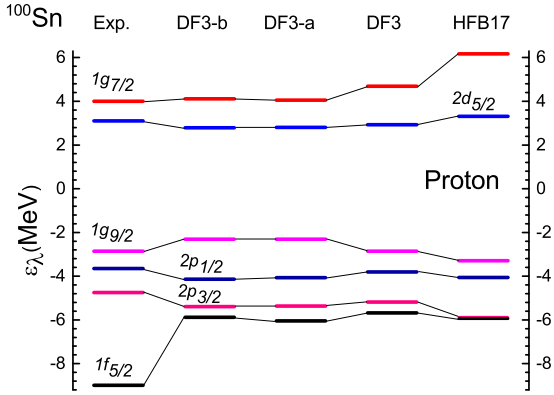

FIG. 10. (Color online) Proton single-particle levels in ^{100}Sn. Experimental values [19] are interpolated from data for neighboring nuclei.

The phonon D function appears in Eq. (16) after connecting two wavy phonon ends in Eq. (17). This corresponds to averaging of the product of two boson (phonon) operators $B_L^+ B_L$ over the ground state of the nucleus with no phonons.

The quantity $\delta_L A$ can be readily obtained by variation of each Green function in the particle-hole propagator A in field g_L induced by the L phonon. The explicit expression for the variation $\delta_L \mathcal{F}$ cannot be found within the TFFS, as in this approach the Landau-Migdal amplitude $\mathcal{F}$ is introduced as a phenomenological quantity. In Ref. [9] the ansatz was proposed,

$$\delta_L \mathcal{F} = \frac{\delta \mathcal{F}(\rho)}{\delta \rho} \delta\rho_L, \quad (18)$$

where

$$\delta\rho_L = A_L g_L \quad (19)$$

is the transition density for excitation of the L phonon.

The complete PC correction from the L phonon to the single-particle energy is

$$\delta\varepsilon_\lambda = Z_\lambda \left(\delta\Sigma^{\rm pole}_{\lambda\lambda} + \delta\Sigma^{\rm tad}_{\lambda\lambda} \right). \quad (20)$$

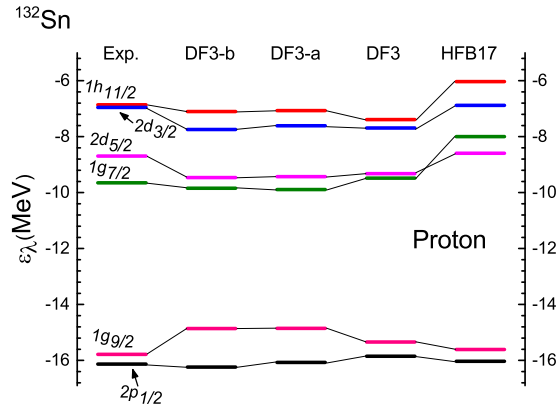

FIG. 12. (Color online) Proton single-particle levels in ^{132}Sn. Experimental data from [19].

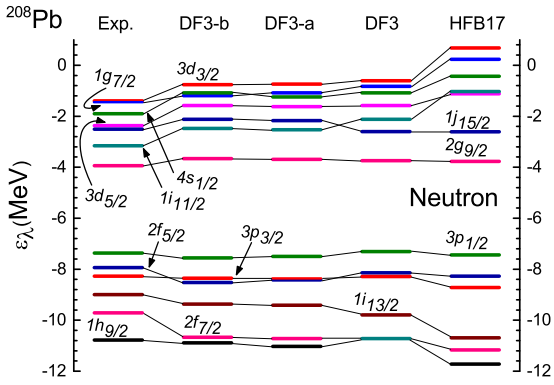

FIG. 13. (Color online) Neutron single-particle levels in ^{208}Pb. Experimental data from [19].

As the term $\delta\Sigma^{\rm tad}$ does not depend on the energy ε, it does not contribute to Z_λ. Hence, the PC contribution to the Z factor is

$$Z_\lambda = \frac{1}{1 - \frac{\partial}{\partial\varepsilon}\delta\Sigma^{\rm pole}_{\lambda\lambda}(\varepsilon)\big|_{\varepsilon=\varepsilon_\lambda}}. \tag{21}$$

The explicit relation for energy derivative of the mass operator, (12), can be easily obtained.

Dealing with the ghost phonon, Eqs. (16) and (17), with the use of (14), can be transformed [9] to

$$\delta\Sigma^{\rm tad}_{L=1} = \frac{\alpha_1^2}{2}\triangle U(r). \tag{22}$$

For the ghost phonon both terms of the sum, (20), are proportional to $\alpha_1^2 \propto 1/\omega_1$, hence the ω_1-even component of Eq. (15) and the tadpole term, (22), should compensate each other:

$$\alpha_1^2 \sum_{\lambda_1 M}\left|\langle\lambda_1|\frac{dU}{dr}Y_{1M}(\mathbf{n})|\lambda\rangle\right|^2 \frac{\varepsilon_\lambda - \varepsilon_{\lambda_1}}{\left(\varepsilon_\lambda - \varepsilon_{\lambda_1}\right)^2 - \omega_1^2} + \left(\delta\Sigma^{\rm tad}_{L=1}\right)_{\lambda\lambda} = 0. \tag{23}$$

This identity could be proved explicitly [9,29] with the use of the identity $(\partial U/\partial\mathbf{r})_{\lambda\lambda'} = (\varepsilon_{\lambda'} - \varepsilon_\lambda)(\partial/\partial\mathbf{r})_{\lambda\lambda'}$.

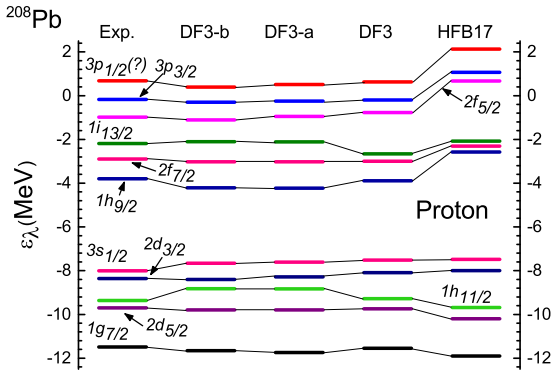

FIG. 14. (Color online) Proton single-particle levels in ^{208}Pb. Experimental data from [19].

TABLE III. Average deviations $\langle\delta\varepsilon_\lambda\rangle_{\rm rms}$ (MeV) of the theory predictions for the single-particle energies from the experimental values for magic nuclei.

Nucleus	N	DF3-b	DF3-a	DF3	HFB17
^{40}Ca	14	1.08	1.25	1.35	1.64
^{48}Ca	12	0.89	1.00	1.01	1.70
^{56}Ni	14	1.00	0.97	0.85	1.40
^{78}Ni	11	1.24	1.41	1.09	1.32
^{100}Sn	13	1.09	1.17	1.01	1.56
^{132}Sn	17	0.58	0.66	0.55	1.15
^{208}Pb	24	0.44	0.51	0.43	1.15
Total	105	0.89	0.98	0.89	1.40

In the result one obtains

$$\delta\varepsilon^{\rm ghost}_\lambda = \frac{1}{2B_1}\sum_{\lambda_1 M}\left|\langle\lambda_1|\frac{dU}{dr}Y_{1M}(\mathbf{n})|\lambda\rangle\right|^2 \times \frac{1 - 2n_{\lambda_1}}{\left(\varepsilon_\lambda - \varepsilon_{\lambda_1}\right)^2 - \omega_1^2}. \tag{24}$$

The physical meaning of the PC correction caused by the ghost 1^- phonon is very simple. This is account for the "recoil effect" due to the center-of-mass (CM) motion. Equation (24), with the use of the above relation for the $(\partial U/\partial\mathbf{r})$ operator, can be reduced to the usual RPA formula for CM motion correction [4],

$$\delta\varepsilon^{\rm ghost}_\lambda = \frac{1}{2B_1}\sum_{\lambda_1 M}\left|\mathbf{k}_{\lambda_1\lambda}\right|^2; \tag{25}$$

although more cumbersome, Eq. (24) is convenient for numerical calculations.

The L-phonon excitation energies ω_L and creation amplitudes $g_L(\mathbf{r})$ were found by solving the self-consistent Eq. (11) with the DF3-a functional. In more detail, the procedure is described in [18]. The results for ω_L and $B(EL)$ values are listed in Table IV. All the L phonons we consider are the surface vibrations which belong to the Goldstone mode corresponding to the spontaneous breaking of the translation symmetry in nuclei [9]. The coordinate form of their creation

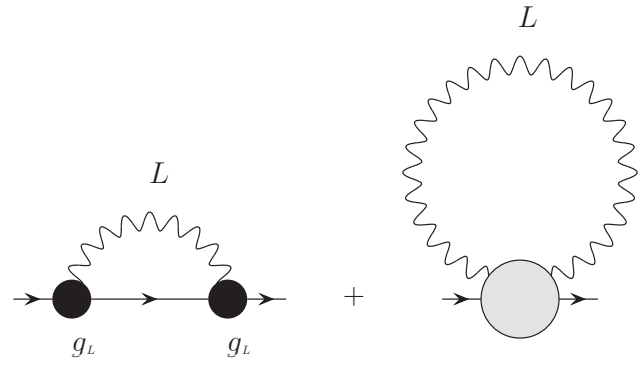

FIG. 15. PC corrections to the mass operator. The gray circle denotes the "tadpole" term.

TABLE IV. Characteristics of the low-lying phonons in magic nuclei, ω_L (MeV) and $B(EL,\mathrm{up})$ ($\mathrm{e}^2\,\mathrm{fm}^{2L}$).

L^π	ω_L^{th}	ω_L^{exp}	$B(EL)^{\mathrm{th}}$	$B(EL)^{\mathrm{exp}}$
			^{40}Ca	
3^-	3.335	3.736 69 (5)	1.52×10^4	1.24×10^4
			^{48}Ca	
2^+	3.576	3.831 72 (6)	0.55×10^2	0.86×10^2
3^-	4.924	4.506 78 (5)	5.701×10^3	0.67×10^4
			^{56}Ni	
2^+	2.826	2.7006 (7)	5.725×10^2	
3^-	8.108	4.932 (3)	2.068×10^4	
			^{78}Ni	
2^+	3.238	–	3.309×10^2	
3^-	6.378	–	1.549×10^4	
			^{100}Sn	
2^+	3.978	–	1.375×10^3	
3^-	5.621	–	1.24×10^5	
			^{132}Sn	
2^+	4.327	4.041 20 (15)	0.104×10^4	$0.11\ (0.03) \times 10^4$
3^-	4.572	4.351 94 (14)	1.29×10^5	
			^{208}Pb	
3^-	2.684	2.615	7.093×10^5	6.12×10^5
5^-_1	3.353	3.198	3.003×10^8	4.47×10^8
5^-_2	3.787	3.708	1.785×10^8	2.41×10^8
2^+_1	4.747	4.086	1.886×10^3	3.18×10^3
2^+_2	5.004	4.928	1.148×10^3	–
4^+_1	4.716	4.324	3.007×10^6	–
4^+_2	5.367	4.911(?)	8.462×10^6	–
6^+_1	4.735	–	6.082×10^9	–
6^+_2	5.429	–	1.744×10^{10}	–

amplitudes $g_L(\mathbf{r})$ is very close to that for the ghost phonon, which is the lowest energy member of this mode:

$$g_L(r) = \alpha_L \frac{dU}{dr} + \chi_L(r), \tag{26}$$

where the in-volume correction $\chi_L(r)$ is rather small. The first, surface term on the right-hand side of Eq. (26) corresponds to the BM model for the surface vibrations [35], the amplitude α_L being related to the dimensionless BM amplitude β_L as $\alpha_L = R\beta_L$, where $R = r_0 A^{1/3}$ is the nucleus radius, and $r_0 = 1.2$ fm.

The smallness of the in-volume component χ_L is demonstrated in Fig. 16 for the 3^-_1 state in ^{208}Pb, which is the most collective one among the surface vibrations in this nucleus. The small spin components $S = 1$ are also displayed. To make them distinguishable, they are multiplied by the factor of 10. The smallness of the spin components is typical for L phonons with a high collectivity. For phonons which are less collective, e.g., the 2^+_1 state in ^{208}Pb, the spin component is more important and should be taken into account. In any case, we always took it into account for all phonons. Similarly, the surface component also dominates in the transition density:

$$\rho_L(r) = \alpha_L \frac{d\rho}{dr} + \eta_L(r). \tag{27}$$

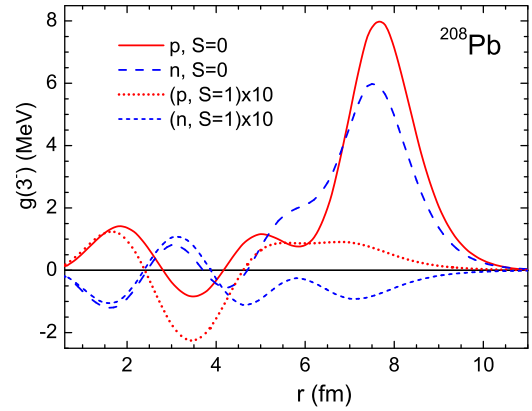

FIG. 16. (Color online) The vertex g_L for the 3^-_1 state in ^{208}Pb.

If one neglects in-volume contributions, the tadpole PC term, (16), can be reduced to a form similar to (16):

$$\delta\Sigma_L^{\mathrm{tad}} = \frac{\alpha_L^2}{2}\frac{2L+1}{3}\triangle U(r). \tag{28}$$

As demonstrated in [29], the in-volume corrections to Eq. (28) are, indeed, small for heavy nuclei, e.g., for ^{208}Pb. At the same time, for light nuclei, e.g., ^{40,48}Ca, the accurate solution [29] of Eq. (17) diminishes the approximate value, (28), for the tadpole term by $\simeq$30%.

Below we neglect the in-volume corrections for all nuclei considered. To find the phonon amplitudes α_L, we used the definition

$$\alpha_L^\tau = \frac{g_L^{\tau,\max}}{\left(\frac{dU}{dr}\right)^{\tau,\max}}, \tag{29}$$

with obvious notation. It should be noted that the values of α_L^n and α_L^p are always very close to each other and to that which follows from the BM model formula for $B(EL)$, $B(EL)_{\mathrm{BM}} = (3Z/4\pi)^2\,\beta_L^2 R^{2L}$ [35], where the dimensionless BM phonon creation amplitude β_L related to that used by us as $\alpha_L = \beta_L R/\sqrt{2L+1}$, $R = 1.2\,A^{1/3}$. For example, for the 3^-_1 state in ^{208}Pb we have $\alpha_L^n = 0.32$ fm, $\alpha_L^p = 0.33$ fm, and $\alpha_L^{\mathrm{BM}} = 0.30$ fm.

Separate contributions of pole and tadpole terms for PC corrections from the first 3^- state to single-particle levels ^{40}Ca are listed in Table V, and those for ^{208}Pb in Table VI. The tadpole correction $\delta\varepsilon_\lambda^{\mathrm{tad}}$ is always positive, whereas the pole one $\delta\varepsilon_\lambda^{\mathrm{pole}}$ is, as a rule, negative. For such cases, these two terms partially cancel each other. In the ^{40}Ca nucleus, these contributions are of the same order, and the sum proves to be positive in almost half of the cases. As mentioned above, the tadpole values in Table V could be reduced by $\simeq$30%, providing the accurate solution [29] of Eq. (17). In ^{208}Pb, the role of the tadpole term is, on average, smaller, but still important. In this case, the in-volume corrections to Eq. (28) are small. Indeed, "the surface-to-volume ratio" decreases as $\propto A^{-1/3}$ for heavy nuclei, therefore the surface vibrations resemble the modes of a classical liquid drop, not penetrating inside its volume.

Consider now the final results of the DF3-a functional for the single-particle spectra for magic nuclei with inclusion of

TABLE V. Pole and tadpole contributions to PC corrections from 3^- states to single-particle energies (MeV) in ^{40}Ca.

λ	$\delta\varepsilon_\lambda^{\rm pole}$	$\delta\varepsilon_\lambda^{\rm tad}$	$\delta\varepsilon_\lambda$
	Neutrons		
$1f_{5/2}$	−0.395	0.592	0.197
$2p_{1/2}$	−0.805	0.305	−0.500
$2p_{3/2}$	−0.833	0.383	−0.450
$1f_{7/2}$	−0.142	0.733	0.591
$1d_{3/2}$	−0.426	0.697	0.271
$2s_{1/2}$	−0.932	0.493	−0.439
$1d_{5/2}$	−0.253	0.731	0.478
	Protons		
$1f_{5/2}$	−0.240	0.470	0.230
$2p_{1/2}$	−0.584	0.152	−0.432
$2p_{3/2}$	−0.224	0.251	0.027
$1f_{7/2}$	0.100	0.677	0.777
$1d_{3/2}$	−0.370	0.659	0.289
$2s_{1/2}$	−0.886	0.429	−0.457
$1d_{5/2}$	−0.234	0.699	0.466

the PC corrections. Let us begin with ^{40}Ca, in Table VII. It also contains the Z_λ factors, which are used in the final expression, (10), for the single-particle energy. The difference $1 - Z_\lambda$ determines the scale of the PC effects. The inequality $1 - Z_\lambda \ll 1$ justifies the validity of the perturbation theory in

TABLE VI. Pole and tadpole contributions to PC corrections from 3^- states to single-particle energies (MeV) in ^{208}Pb.

λ	$\delta\varepsilon_\lambda^{\rm pole}$	$\delta\varepsilon_\lambda^{\rm tad}$	$\delta\varepsilon_\lambda$
	Neutrons		
$3d_{3/2}$	−0.150	0.012	−0.137
$2g_{7/2}$	−0.142	0.061	−0.081
$4s_{1/2}$	−0.134	0.016	−0.118
$3d_{5/2}$	−0.147	0.023	−0.124
$1j_{15/2}$	−0.708	0.204	−0.504
$1i_{11/2}$	−0.058	0.198	0.140
$2g_{9/2}$	−0.244	0.076	−0.167
$3p_{1/2}$	−0.220	0.053	−0.167
$2f_{5/2}$	−0.186	0.094	−0.092
$3p_{3/2}$	−0.205	0.056	−0.149
$1i_{13/2}$	0.057	0.211	0.269
$2f_{7/2}$	0.724	0.091	0.815
$1h_{9/2}$	−0.014	0.197	0.184
	Protons		
$3p_{1/2}$	−0.375	0.153	−0.222
$3p_{3/2}$	−0.371	0.152	−0.219
$2f_{5/2}$	−0.278	0.168	−0.110
$1i_{13/2}$	−0.534	0.266	−0.268
$2f_{7/2}$	−0.409	0.168	−0.240
$1h_{9/2}$	−0.054	0.222	0.168
$3s_{1/2}$	−0.310	0.143	−0.167
$2d_{3/2}$	−0.241	0.146	−0.095
$1h_{11/2}$	−0.017	0.246	0.229
$2d_{5/2}$	0.435	0.147	0.582
$1g_{7/2}$	−0.271	0.197	−0.074

TABLE VII. PC corrections to single-particle energies (MeV) in ^{40}Ca.

λ	Z_λ	$\varepsilon_\lambda^{(0)}$	$\delta\varepsilon_\lambda$		ε_λ	$\varepsilon_\lambda^{\rm exp}$ [19]
			3^-	1^-		
			Neutrons			
$1f_{5/2}$	0.947	−2.124	0.197	0.321	−1.634	−2.65
$2p_{1/2}$	0.934	−3.729	−0.500	0.133	−4.072	−4.42
$2p_{3/2}$	0.916	−5.609	−0.450	0.130	−5.902	−6.42
$1f_{7/2}$	0.947	−9.593	0.591	0.173	−8.870	−8.36
$1d_{3/2}$	0.965	−14.257	0.271	0.267	−13.738	−15.64
$2s_{1/2}$	0.930	−15.780	−0.439	0.184	−16.017	−18.11
$1d_{5/2}$	0.969	−19.985	0.478	0.224	−19.305	−21.27
			Protons			
$1f_{5/2}$	0.963	4.359	0.230	0.300	4.869	4.60
$2p_{1/2}$	0.950	2.456	−0.432	0.062	2.104	2.38
$2p_{3/2}$	0.966	0.936	0.027	0.091	1.050	0.63
$1f_{7/2}$	0.960	−2.678	0.777	−0.198	−2.122	−1.09
$1d_{3/2}$	0.966	−7.264	0.289	0.262	−6.733	−8.33
$2s_{1/2}$	0.931	−8.663	−0.457	0.170	−8.931	−10.85
$1d_{5/2}$	0.969	−12.856	0.466	0.216	−12.196	−13.73

g_L^2. In addition to the 3^- state, Table VII lists the corrections due to the recoil effect from the spurious 1^- state. For this nucleus, the latter is significant: for several states, comparable with that from the 3^- state. The agreement of the PC corrections with the data is a little worse. Now the total average error is 1.30 MeV, compared to the 1.25 MeV without PC corrections. The main reason for this disagreement is the overestimate of the tadpole term discussed above.

In ^{48}Ca (Table VIII) there are two states, $1f^n_{5/2}$ and $1d^p_{5/2}$, with anomalously small values of Z_λ. This occurs because of the occasional smallness of one of the denominators in Eq. (12) due to some semigeneration of the energies ε_λ and $\varepsilon_\lambda \pm \omega_L$. Of course, in this situation the plain perturbation theory is not valid. An improved approach should be developed with

TABLE VIII. PC corrections to single-particle energies (MeV) in ^{48}Ca.

λ	Z_λ	$\varepsilon_\lambda^{(0)}$	$\delta\varepsilon_\lambda$			ε_λ	$\varepsilon_\lambda^{\rm exp}$ [19]
			3^-	2^+	1^-		
			Neutrons				
$1g_{9/2}$	0.796	0.836	0.438	−0.069	0.068	1.184	0.45
$1f_{5/2}$	0.164	−0.508	–	–	–	−0.508	−1.20
$2p_{1/2}$	0.773	−3.890	−0.095	−0.457	0.098	−4.241	−3.12
$2p_{3/2}$	0.939	−5.784	−0.116	−0.068	0.119	−5.846	−5.15
$1f_{7/2}$	0.965	−9.488	0.153	0.095	0.121	−9.132	−9.95
			Protons				
$1f_{5/2}$	0.873	−4.048	0.076	−0.330	0.249	−4.052	−4.55
$2p_{1/2}$	0.648	−3.549	−0.114	−1.399	0.157	−4.427	−5.05
$2p_{3/2}$	0.604	−4.731	−0.089	0.390	0.126	−4.473	−6.55
$1f_{7/2}$	0.899	−9.909	0.144	−0.305	0.176	−9.896	−9.63
$1d_{3/2}$	0.917	−16.172	0.099	0.369	0.190	−15.568	−15.81
$2s_{1/2}$	0.915	−15.098	−0.024	0.476	0.147	−14.550	−16.17
$1d_{5/2}$	0.116	−19.913	–	–	–	−19.913	−21.58

TABLE IX. PC corrections to single-particle energies (MeV) in ^{56}Ni.

λ	Z_λ	$\varepsilon_\lambda^{(0)}$	$\delta\varepsilon_\lambda$			ε_λ	$\varepsilon_\lambda^{\exp}$ [19]
			3^-	2^+	1^-		
Neutrons							
$1g_{9/2}$	0.777	−5.311	−0.263	−0.120	0.097	−5.533	−6.55
$2p_{1/2}$	0.774	−9.615	−0.101	−0.411	0.149	−9.895	−9.14
$1f_{5/2}$	0.008	−8.258	–	–	–	−8.258	−9.48
$2p_{3/2}$	0.933	−11.064	−0.111	−0.042	0.126	−11.089	−10.25
$1f_{7/2}$	0.945	−15.588	0.309	0.130	0.137	−15.044	−16.65
$1d_{3/2}$	0.927	−20.763	0.424	0.141	0.148	−20.103	−19.84
$2s_{1/2}$	0.752	−20.911	0.800	0.180	0.120	−20.084	−20.40
Protons							
$1g_{9/2}$	0.809	3.722	−0.224	−0.054	0.084	3.565	2.77
$2p_{1/2}$	0.761	−0.648	−0.106	−0.491	0.122	−1.011	0.37
$1f_{5/2}$	0.445	0.713	0.205	−0.307	0.215	0.763	0.29
$2p_{3/2}$	0.911	−1.905	−0.119	−0.123	0.106	−2.029	−0.74
$1f_{7/2}$	0.963	−6.276	0.280	0.178	0.129	−5.711	−7.16
$1d_{3/2}$	0.941	−11.432	0.388	0.217	0.145	−10.726	−10.08
$2s_{1/2}$	0.815	−11.349	0.659	0.101	0.111	−10.639	−10.72

exact diagonalization of the "two-level" problem. Fortunately, such cases are very rare: two for ^{48}Ca, one for ^{56}Ni, and one for ^{208}Pb. Therefore we postpone the solution of this problem, skipping the calculation of the energy corrections $\delta\varepsilon_\lambda$ for these states. They are reported in Tables VIII, IX, and XIII to call attention to this problem. For the ^{48}Ca nucleus the phonon 2^+ is added, as sometimes its contribution exceeds that of the 3^- state. The contribution of the recoil effect is less than in ^{40}Ca but still important. It should be noted that a rough estimate of this effect is $\simeq\varepsilon_F/A$, so it becomes small for heavy nuclei but, as a rule, not negligible. We have included it for all nuclei, as it is, in fact, model independent.

For all nuclei from ^{56}Ni to ^{132}Sn (Tables IX–XII), the set of phonons we take into account is the same as for ^{48}Ca, i.e., 3^-, 2^+ and the ghost 1^- state. For all of them the contributions

TABLE X. PC corrections to single-particle energies (MeV) in ^{78}Ni.

λ	Z_λ	$\varepsilon_\lambda^{(0)}$	$\delta\varepsilon_\lambda$			ε_λ	$\varepsilon_\lambda^{\exp}$ [19][a]
			3^-	2^+	1^-		
Neutrons							
$3s_{1/2}$	0.873	−1.045	−0.080	−0.409	0.017	−1.457	−1.44
$2d_{5/2}$	0.915	−1.477	−0.040	−0.162	0.052	−1.615	−1.98
$1g_{9/2}$	0.918	−5.481	0.169	0.264	0.068	−5.021	−5.86
$2p_{1/2}$	0.910	−8.268	−0.059	0.349	0.083	−7.929	−7.21
$1f_{5/2}$	0.912	−8.553	0.172	0.364	0.114	−7.960	−8.39
$1p_{3/2}$	0.724	−9.641	0.446	0.378	0.054	−9.005	−8.54
Protons							
$1g_{9/2}$	0.773	−11.138	−0.190	−0.152	0.099	−11.326	−8.91
$2p_{1/2}$	0.679	−14.185	−0.104	−0.811	0.125	−14.721	−12.04
$2p_{3/2}$	0.880	−15.526	−0.115	−0.161	0.102	−15.680	−13.44
$1f_{5/2}$	0.927	−15.061	0.168	−0.081	0.125	−14.864	−14.94
$1f_{7/2}$	0.943	−20.245	0.214	0.195	0.112	−19.754	−20.06

[a]Experimental values are interpolated from data for neighboring nuclei.

TABLE XI. PC corrections to single-particle energies (MeV) in ^{100}Sn.

λ	Z_λ	$\varepsilon_\lambda^{(0)}$	$\delta\varepsilon_\lambda$			ε_λ	$\varepsilon_\lambda^{\exp}$ [19][a]
			3^-	2^+	1^-		
Neutrons							
$1h_{11/2}$	0.755	−7.630	−0.314	−0.142	0.061	−7.928	−7.78
$2d_{3/2}$	0.810	−9.087	−0.097	−0.568	0.083	−9.559	−9.48
$3s_{1/2}$	0.661	−9.158	−0.194	−0.977	0.060	−9.893	−9.58
$2d_{5/2}$	0.899	−11.180	−0.121	−0.152	0.058	−11.374	−11.05
$1g_{7/2}$	0.928	−9.705	0.193	−0.129	0.100	−9.552	−11.13
$1g_{9/2}$	0.938	−16.449	0.268	0.199	0.077	−15.939	−17.48
$2p_{1/2}$	0.941	−18.432	−0.068	0.232	0.074	−18.209	−17.94
Protons							
$1g_{7/2}$	0.930	4.077	0.206	−0.132	0.097	4.237	4.00
$2d_{5/2}$	0.908	2.812	−0.136	−0.143	0.044	2.599	3.10
$1g_{9/2}$	0.938	−2.345	0.256	0.196	0.072	−1.853	−2.86
$2p_{1/2}$	0.942	−4.081	−0.072	0.221	0.068	−3.877	−3.65
$2p_{3/2}$	0.750	−5.360	0.647	0.275	0.050	−4.631	−4.75
$1f_{5/2}$	0.891	−6.030	0.276	0.299	0.074	−5.451	−8.99

[a]Experimental values are interpolated from data for neighboring nuclei.

of the 3^- and 2^+ phonons are of the same order of magnitude, whereas the 1^- contribution diminishes in accordance with the above estimate. For ^{208}Pb we calculated the contributions of nine phonons: 3^-, $5^-_{1,2}$, $2^+_{1,2}$, $4^+_{1,2}$, and $2^+_{1,2}$. As a rule, the contribution of the 3^--phonon dominates. However, sometimes the contribution of all other phonons is comparable with that of 3^-. For this nucleus, the PC corrections improve the description of the single-particle spectrum. The average error is now 0.34 MeV instead of 0.51 MeV.

TABLE XII. PC corrections to single-particle energies (MeV) in ^{132}Sn.

λ	Z_λ	$\varepsilon_\lambda^{(0)}$	$\delta\varepsilon_\lambda$			ε_λ	$\varepsilon_\lambda^{\exp}$[19]
			3^-	2^+	1^-		
Neutrons							
$1i_{13/2}$	0.734	0.745	−0.368	−0.085	0.032	0.436	0.25
$2f_{5/2}$	0.927	−0.255	−0.076	−0.224	0.025	−0.510	−0.44
$3p_{1/2}$	0.942	−0.629	−0.117	−0.187	−0.001	−0.916	−0.79
$1h_{9/2}$	0.942	0.192	0.119	−0.112	0.080	0.274	−0.88
$3p_{3/2}$	0.919	−1.095	−0.100	−0.234	0.011	−1.392	−1.59
$2f_{7/2}$	0.938	−2.319	−0.084	−0.084	0.029	−2.449	−2.45
$2d_{3/2}$	0.945	−8.044	−0.080	0.177	0.051	−7.904	−7.39
$1h_{11/2}$	0.948	−7.472	0.215	0.135	0.047	−7.096	−7.63
$3s_{1/2}$	0.939	−8.159	−0.120	0.201	0.029	−8.056	−7.72
$2d_{5/2}$	0.727	−9.993	0.619	0.206	0.031	−9.371	−9.04
$1g_{7/2}$	0.942	−9.620	0.173	0.193	0.059	−9.220	−9.82
Protons							
$1h_{11/2}$	0.832	−7.056	−0.174	−0.044	0.056	−7.190	−6.86
$2d_{3/2}$	0.858	−7.606	−0.104	−0.304	0.065	−7.900	−6.95
$2d_{5/2}$	0.921	−9.420	−0.153	−0.063	0.048	−9.576	−8.69
$1g_{7/2}$	0.967	−9.892	0.182	−0.010	0.063	−9.665	−9.65
$1g_{9/2}$	0.963	−14.842	0.221	0.094	0.062	−14.479	−15.78
$2p_{1/2}$	0.963	−16.073	−0.059	0.100	0.052	−15.983	−16.13

TABLE XIII. PC corrections to single-particle energies (MeV) in ^{208}Pb.

λ	Z_λ	$\varepsilon_\lambda^{(0)}$	$\delta\varepsilon_\lambda$					ε_λ	$\varepsilon_\lambda^{\rm exp}$ [19]
			3^-	5_1^-	2_1^+	$\sum_{\rm rest}$	1^-		
					Neutrons				
$3d_{3/2}$	0.879	−0.709	−0.137	−0.027	−0.086	−0.278	0.004	−1.171	−1.40
$2g_{7/2}$	0.886	−1.091	−0.081	−0.013	−0.095	−0.215	0.026	−1.426	−1.45
$4s_{1/2}$	0.895	−1.080	−0.118	−0.028	−0.066	−0.240	0.003	−1.483	−1.90
$3d_{5/2}$	0.873	−1.599	−0.124	−0.034	−0.104	−0.234	0.009	−2.023	−2.37
$1j_{15/2}$	0.618	−2.167	−0.504	−0.016	−0.025	0.009	0.025	−2.483	−2.51
$1i_{11/2}$	0.945	−2.511	0.140	0.022	−0.030	0.023	0.041	−2.327	−3.16
$2g_{9/2}$	0.882	−3.674	−0.167	−0.005	−0.032	−0.097	0.018	−3.924	−3.94
$3p_{1/2}$	0.926	−7.506	−0.167	−0.033	0.074	0.058	0.022	−7.549	−7.37
$2f_{5/2}$	0.923	−8.430	−0.092	−0.006	0.066	0.124	0.032	−8.316	−7.94
$3p_{3/2}$	0.913	−8.363	−0.149	0.004	0.081	0.074	0.016	−8.338	−8.27
$1i_{13/2}$	0.902	−9.411	0.269	0.052	0.054	0.154	0.032	−8.905	−9.00
$2f_{7/2}$	0.567	−10.708	0.815	0.023	0.098	0.190	0.020	−10.059	−9.71
$1h_{9/2}$	0.892	−11.009	0.184	0.021	0.070	0.223	0.033	−10.535	−10.78
					Protons				
$3p_{1/2}$	0.005	0.484	–	–	–	–	–	0.484	0.68
$3p_{3/2}$	0.690	−0.249	−0.219	−0.100	−0.154	−0.365	0.026	−0.810	−0.17
$2f_{5/2}$	0.812	−0.964	−0.110	−0.016	−0.106	−0.248	0.036	−1.325	−0.98
$1i_{13/2}$	0.741	−2.082	−0.268	0.012	−0.021	0.039	0.034	−2.234	−2.19
$2f_{7/2}$	0.859	−3.007	−0.240	−0.014	−0.013	−0.095	0.025	−3.298	−2.90
$1h_{9/2}$	0.958	−4.232	0.168	0.023	0.007	0.052	0.035	−3.959	−3.80
$3s_{1/2}$	0.929	−7.611	−0.167	0.018	0.048	0.051	0.026	−7.633	−8.01
$2d_{3/2}$	0.937	−8.283	−0.095	0.006	0.052	0.068	0.031	−8.223	−8.36
$1h_{11/2}$	0.931	−8.810	0.229	0.021	0.020	0.134	0.037	−8.399	−9.36
$2d_{5/2}$	0.711	−9.782	0.582	0.006	0.043	0.113	0.024	−9.234	−9.70
$1g_{7/2}$	0.423	−11.735	−0.074	0.056	0.087	0.190	0.029	−11.613	−11.49

The average deviations $\langle\delta\varepsilon_\lambda\rangle_{\rm rms}$ for all nuclei we consider for the DF3-a functional, with and without PC corrections, are presented in Table XIV. For lighter nuclei, $A = 40 \div 100$, PC corrections worsen the agreement a bit, with the only exception of ^{78}Ni. For heavy nuclei, ^{132}Sn and ^{208}Pb, the agreement becomes better.

To conclude this section, we compare in Table XV our results for ^{208}Pb with predictions of the RMF theory [27], the only calculation we know where PC corrections to the single-particle spectrum are found self-consistently. In this calculation only the pole diagram in Fig. 8 is taken into account. It is seen that the agreement of our result with the data is significantly better. For the RMF spectrum the average deviation from the data is $\langle\delta\varepsilon_\lambda\rangle_{\rm rms} = 0.81$ MeV, which is two times worse than the result of the DF3-a functional with PC corrections.

TABLE XIV. PC effect on average deviations $\langle\delta\varepsilon_\lambda\rangle_{\rm rms}$ (MeV) of the theory predictions for single-particle energies from the experimental values for the DF3-a functional.

Nucleus	N	DF3-a + ph	DF3-a
^{40}Ca	14	1.30	1.25
^{48}Ca	12	1.08	1.00
^{56}Ni	14	0.98	0.97
^{78}Ni	11	1.34	1.41
^{100}Sn	13	1.21	1.17
^{132}Sn	17	0.60	0.66
^{208}Pb	24	0.34	0.51
Total	105	0.97	0.98

IV. CONCLUSION

Single-particle spectra of seven magic nuclei, from ^{40}Ca to ^{208}Pb, some of which have become available recently [19], are described within the EDF method of Fayans *et al*. Comparison is made with the predictions of the SHF method with the functional HFB-17, the record holder in describing nuclear masses among self-consistent approaches. Three versions of the Fayans functional are used, DF3 [16] and two options, DF3-a and DF3-b, with different spin-orbit parameter values. One of these, DF3-a, was suggested in [30] to describe nuclei heavier than lead. The second option, DF3-b, is found in this paper to give a better description of the spin-orbit differences Δ_{nls}. The bulk of the data [19] provides 35 such differences, which makes it possible to find the optimal set of spin-orbit parameters. The DF3-b set is the most successful: the average deviation from experimental values $\langle\delta\Delta_{nls}\rangle_{\rm rms}$ is equal to 0.60 MeV. For comparison, it is 0.68 MeV for the DF3-a functional, about 1 MeV for the original DF3 functional, and more than 2 MeV for the HFB-17 functional.

Description of the single-particle energies for all three versions of the DF3 functional is also significantly better than for the HFB-17 functional. To compare the accuracy of

TABLE XV. Single-particle energies (MeV) with PC corrections in ^{208}Pb. Comparison with predictions of the RMF theory [27].

λ	ε_λ[DF3 − a + ph]	$\varepsilon_\lambda^{\rm exp}$ [19]	ε_λ[RMF + ph]
	Neutrons		
$3d_{3/2}$	−1.171	−1.40	−0.63
$2g_{7/2}$	−1.426	−1.45	−1.14
$4s_{1/2}$	−1.483	−1.90	−0.92
$3d_{5/2}$	−2.023	−2.37	−1.39
$1j_{15/2}$	−2.483	−2.51	−1.84
$1i_{11/2}$	−2.327	−3.16	−3.30
$2g_{9/2}$	−3.924	−3.94	−3.29
$3p_{1/2}$	−7.549	−7.37	−7.68
$2f_{5/2}$	−8.316	−7.94	−8.66
$3p_{3/2}$	−8.338	−8.27	−8.26
$1i_{13/2}$	−8.905	−9.00	−9.10
$2f_{7/2}$	−10.059	−9.71	−9.71
$1h_{9/2}$	−10.535	−10.78	−11.96
	Protons		
$3p_{1/2}$	0.484	0.68	1.09
$3p_{3/2}$	−0.810	−0.17	−0.16
$2f_{5/2}$	−1.325	−0.98	−1.07
$1i_{13/2}$	−2.234	−2.19	−2.49
$2f_{7/2}$	−3.298	−2.90	−2.87
$1h_{9/2}$	−3.959	−3.80	−5.04
$3s_{1/2}$	−7.633	−8.01	−8.41
$2d_{3/2}$	−8.223	−8.36	−9.33
$1h_{11/2}$	−8.399	−9.36	−9.92
$2d_{5/2}$	−9.234	−9.70	−10.05
$1g_{7/2}$	−11.613	−11.49	−13.74
$\langle\delta\varepsilon_\lambda\rangle_{\rm rms}$	0.34		0.81

different theories, on average, we found the average differences $\langle\delta\varepsilon_\lambda\rangle_{\rm rms}$ between theoretical and experimental values of the single-particle energies ε_λ. These quantities are found for each nucleus and for the whole set of 105 levels. For each of the nuclei under consideration the predictions of the Fayans functional are more accurate. For example, for ^{40}Ca, $\langle\delta\varepsilon_\lambda\rangle_{\rm rms}$ values are equal to 1.08-1.35 MeV for the three versions of the DF3 functional and 1.64 MeV for the HFB-17 functional. For the ^{208}Pb nucleus, the advantage of the Fayans functional is even more pronounced; the corresponding values of $\langle\delta\varepsilon_\lambda\rangle_{\rm rms}$ are 0.43–0.51 MeV for the DF3 functionals and 1.15 MeV for the HFB-17 one. As for the overall values of $\langle\delta\varepsilon_\lambda\rangle_{\rm rms}$, they are equal to 0.89 MeV for the DF3 functional, 0.98 MeV for the DF3-a functional, and 0.89 MeV for DF3-b. For the HFB-17 functional it is equal to 1.40 MeV.

Thus, all three versions of the DF3 functional describe the single-particle levels with an accuracy of, on average, better than 1 MeV. We explain this by two main features of the Fayans EDF. First, the Fayans EDF uses the bare mass, $m^* = m$, prescription of the Kohn-Sham method. The self-consistent TFFS [9]—which takes into account not only the momentum dependence, as does the SHF method, but also the energy dependence effects—leads to a result which is rather close to the Kohn-Sham prescription. This occurs due to the strong, almost-exact cancellation of the so-called k mass and E mass. The latter appears due to the energy dependence of the quasiparticle mass operator on energy, which has no analog in the SHF method. Second, the density dependence of the Fayans EDF is much more sophisticated than that of the SHF one. This is also an implicit consequence of the energy dependence effects taken into account in the TFFS. In our opinion, the reason why the HFB-17 functional, which describes nuclear masses perfectly well, is less accurate for single-particle spectra is that the density dependence of SHF functionals is oversimplified for describing more delicate nuclear characteristics.

The self-consistent description of the PC corrections to single-particle spectra in magic nuclei is another subject of this paper. Calculations are carried out for the DF3-a functional, which was successful in describing the excitation energies and $B(E2)$ values [18,31], as well as the quadrupole moments [32,33], in semimagic nuclei. The method developed in [9] and [29] is used, which permits us to calculate PC contributions not only from the usual pole diagram but also from the tadpole one. The latter is taken into account approximately, with ansatz (28), which neglects the in-volume components of the vertices $g_L(r)$ of the surface vibrations. As shown in [29], this approximation works well for heavy nuclei but it is questionable for lighter ones. The tadpole contribution is almost always positive as long as the pole contribution is usually negative. As a result, the two terms, pole and tadpole, usually cancel each other and the absolute value of the sum is less than that from the pole diagram alone. The contribution to ε_λ from the spurious 1^- state, which describes the recoil effect due to the CM motion, is also taken into account. It is very important for lighter nuclei but rather minor for ^{208}Pb. After accounting for the PC effects the average description of single-particle spectra becomes a little worse for light nuclei but definitely better for heavy nuclei. For example. for ^{208}Pb we obtained an average error equal to 0.34 MeV, versus 0.51 MeV without PC corrections. As for overall accuracy, the deviations of the theoretical predictions for single-particle energies ε_λ from the experimental values $\langle\delta\varepsilon_\lambda\rangle_{\rm rms}$ averaged over more than 100 states are 0.97 and 0.98 MeV with and without PC corrections, respectively. To improve the accuracy for light nuclei, it is necessary to find the tadpole termtaking into account exactly the in-volume contributions.

ACKNOWLEDGMENTS

This work was partly supported by Grant No. NSh-932.2014.2 from the Russian Ministry for Science and Education and by RFBR Grant Nos. 12-02-00955-a, 13-02-00085-a, 13-02-12106-ofi_m, 14-02-00107-a, and 14-02-31353-mol_a and Grant IN2P3-RFBR under Agreement No. 110291054.

[1] D. Vautherin and D. M. Brink, Phys. Rev. C **5**, 626 (1972).

[2] A. B. Migdal, *Theory of Finite Fermi Systems and Applications to Atomic Nuclei* (Nauka, Moscow, 1965); *Theory of Finite Fermi Systems and Applications to Atomic Nuclei* (Wiley, New York, 1967).

[3] P. Hohenberg and W. Kohn, Phys. Rev. **136**, B864 (1964).

[4] P. Ring and P. Schuck, *The Nuclear Many-Body Problem* (Springer, Berlin, 1980).
[5] S. Goriely, N. Chamel, and J. M. Pearson, Phys. Rev. Lett. **102**, 152503 (2009).
[6] B. A. Brown, Phys. Rev. C **58**, 220 (1998).
[7] S. A. Fayans and V. A. Khodel, Zh. Eksp. Teor. Fiz. **17**, 633 (1973) [JETP Lett. **17**, 444 (1973)].
[8] E. E. Saperstein and V. A. Khodel, Zh. Eksp. Teor. Fiz. **81**, 22 (1981) [JETP **54**, 12 (1981)].
[9] V. A. Khodel and E. E. Saperstein, Phys. Rep. **92**, 183 (1982).
[10] A. B. Migdal, *Theory of Finite Fermi Systems and Applications to Atomic Nuclei*, 2nd ed. (Nauka, Moscow, 1983).
[11] M. Jaminon and C. Mahaux, Phys. Rev. C **41**, 697 (1990).
[12] V. A. Khodel, Zh. Eksp. Teor. Fiz. **16**, 410 (1972) [JETP Lett. **16**, 291 (1972)]; **18**, 126 (1973); Sov. J. Nucl. Phys. **19**, 376 (1974).
[13] V. A. Khodel, E. E. Saperstein, and M. V. Zverev, Nucl. Phys. A **465**, 397 (1987).
[14] W. Kohn and L. J. Sham, Phys. Rev. **140**, A1133 (1965).
[15] A. V. Smirnov, S. V. Tolokonnikov, and S. A. Fayans, Sov. J. Nucl. Phys. **48**, 995 (1988).
[16] D. J. Horen, G. R. Satchler, S. A. Fayans, and E. L. Trykov, Nucl. Phys. A **600**, 193 (1996); I. N. Borzov, S. A. Fayans, Q. E. Krömer, and D. Zawischa, Z. Phys. A **335**, 117 (1996).
[17] S. A. Fayans, S. V. Tolokonnikov, E. L. Trykov, and D. Zawischa, Nucl. Phys. A **676**, 49 (2000).
[18] S. V. Tolokonnikov, S. Kamerdzhiev, D. Voitenkov, S. Krewald, and E. E. Saperstein, Phys. Rev. C **84**, 064324 (2011).
[19] H. Grawe, K. Langanke, and G. Martínez-Pinedo, Rep. Prog. Phys. **70**, 1525 (2007).
[20] V. G. Soloviev, *Theory of Complex Nuclei* (Pergamon Press, Oxford, 1976).
[21] R. A. Broglia, R. Liotta, and V. Paar, Phys. Lett. B **38**, 480 (1972).
[22] V. Bernard and v. G. Nguyen, Nucl. Phys. A **348**, 75 (1980).
[23] A. P. Severyukhin, V. V. Voronov, and N. V. Giai, Phys. Rev. C **77**, 024322 (2008).
[24] F. Barranco, R. A. Broglia, G. Colo *et al*., Eur. Phys. J. A **21**, 57 (2004).
[25] A. Pastore, F. Barranco, R. A. Broglia, and E. Vigezzi, Phys. Rev. C **78**, 024315 (2008).
[26] L.-G. Cao, G. Colò, H. Sagawa, and P. F. Bortignon, arXiv:1401.1983v1 [nucl-th].
[27] E. Litvinova and P. Ring, Phys. Rev. C **73**, 044328 (2006).
[28] P. Ring, Prog. Part. Nucl. Phys. **37**, 193 (1996).
[29] A. P. Platonov, Sov. J. Nucl. Phys. **34**, 612 (1981).
[30] S. V. Tolokonnikov and E. E. Saperstein, Phys. At. Nucl. **73**, 1684 (2010).
[31] S. V. Tolokonnikov, S. Kamerdzhiev, S. Krewald, E. E. Saperstein, and D. Voitenkov, EPJ Web Conf. **38**, 04002 (2012).
[32] S. V. Tolokonnikov, S. Kamerdzhiev, S. Krewald, E. E. Saperstein, and D. Voitenkov, EPJA **48**, 70 (2012).
[33] S. Kamerdzhiev, S. Krewald, S. Tolokonnikov, E. E. Saperstein, and D. Voitenkov, EPJ Web Conf. **38**, 10002 (2012).
[34] A. Bohr and B. R. Mottelson, *Nuclear Structure* (Benjamin, New York, 1969), Vol. 1.
[35] A. Bohr and B. R. Mottelson, *Nuclear Structure* (Benjamin, New York, 1974), Vol. 2.